SCIENCE CHINA
Chemistry

•ARTICLES•

August 2025 Vol.68 No.8: 3586–3594
https://doi.org/10.1007/s11426-024-2520-y

Intramolecular direct arylation through mechanochemistry: efficient synthesis of corannulene-based *peri*-annulated curved nanographenes

Zhongbo Zhang[1] & Mihaiela C. Stuparu[1,2*]

[1]*School of Chemistry, Chemical Engineering and Biotechnology, Nanyang Technological University, Singapore 637371, Singapore*
[2]*National Institute for Research and Development of Isotopic and Molecular Technologies-INCDTIM, Cluj-Napoca 400293, Romania*

Received November 28, 2024; accepted January 8, 2025; published online February 6, 2025

Peri-annulation is recognized as an influential structural motif in accessing functional molecular materials. However, efficient synthetic access to *peri*-annulated structures remains challenging. Herein, we show that mechanochemistry is a valuable synthetic tool to achieve this goal. It is comparatively better than activation through microwave irradiation and conventional solution-phase reactions. The synthesized materials are molecularly curved nanographenes containing sulfur and selenium atoms. The curvature comes from the use of corannulene as the central building block, upon which the benzothiophene or benzoselenophene are *peri*-annulated through the palladium-catalyzed direct arylation reactions. *Peri*-annulation endows the nanographene structures with better optical properties as compared to other annulation chemistries.

direct arylation, mechanochemistry, nanographenes, *peri*-annulation, zigzag edge

Citation: Zhang Z, Stuparu MC. Intramolecular direct arylation through mechanochemistry: efficient synthesis of corannulene-based *peri*-annulated curved nanographenes. *Sci China Chem*, 2025, 68: 3586–3594, https://doi.org/10.1007/s11426-024-2520-y

1 Introduction

Mechanochemistry drives chemical reactions by utilizing mechanical forces generated by the collision of metal balls on the walls of a metal jar in a milling machine [1]. Typically, such reactions are carried out in the solid state. In the synthesis of organic molecules and materials, thus, it brings sustainability through the omission of toxic and hazardous organic solvents from the system. The benefits of mechanochemistry, however, are not limited to enhancing the green metrics of a reaction. The unique mixing and milling actions may lead to new reaction pathways and products [2]. For instance, high-energy conditions achieved through shear and impact forces can bend molecules in unnatural geometries which can be trapped to prepare curved aromatic structures in an efficient manner [3]. Scalability is another beneficial attribute [4]. In the past decade, thus, this synthetic technique has caught the imagination of the scientific community and a number of sophisticated advances have been made. For instance, parallel and continuous synthesis [5], rapid mixing techniques [6], direct mechanocatalysis [7], and liquid-assisted grinding have been established [8]. A control over reaction parameters such as temperature is developed [9]. The feasibility and significance of gas-phase milling is established [10]. In terms of material classes, mechanochemistry has significantly impacted the research area of polycyclic aromatic hydrocarbons and π-conjugated materials since mechanochemical reactions are not constrained by material solubility, an issue typically encountered in the synthesis of polyarenes [11,12].

Nanographenes are molecularly precise fragments of gra-

Published in virtual special issue “Chemistry Research in Singapore”
*Corresponding author (email: mstuparu@ntu.edu.sg)

phene with potential optoelectronic applications [13]. One method to obtain such nanostructures is through aromatic area enlargement of a core molecule [14]. Such π-extensions can occur at the bay (concave armchair edges), *K* (convex armchair edges), and/or *L* (zigzag edges) regions (Figure 1). π-Extensions at the bay (*ortho*-*ortho*-annulation) and *K* (*ortho*-annulation) regions are common. The examples of aromatic area extension through the zigzag edge (*peri*-annulation) are uncommon [15–17]. In considering bowl-shaped nanographenes based on a corannulene core, Scott's palladium-catalyzed microwave irradiation method is the most valuable [16a–c,17]. It produces structures more curved than fullerene C_{60} with the help of annulations through 5-membered rings [16a]. In the case of annulations through six-membered rings, Würthner and coworkers [15h] established palladium-catalyzed annulations using naphthalene imide precursors. Under Scholl-type conditions, *peri*-annulations through five or six-membered rings remain challenging [12n].

In understanding the effect of *peri*-annulation on molecular properties, the rylene series represents a good example that is prepared through *peri*-annulations of naphthylenes [18]. Rylenes are more stable than acenes. Rylenes also display a comparatively lower band gap than the fully benzenoid polyarenes [19]. Thus, *peri*-annulated nanographenes become a significant goal in nanographene chemistry. Mechanochemistry, with its many beneficial attributes, becomes a natural choice in synthetic access explorations of such challenging structures. However, thus far, studies in this regard remain rare [12n]. Towards this end, in this work, we compare different synthetic methods: (1) traditional oil-bath heating in a solution-phase reaction, (2) microwave irradiation, and (3) mechanochemical activation. The results indicate that mechanochemistry is superior to the solution phase and microwave radiation chemistries for *peri*-annulation purposes (see Supporting Information online for details).

2 Results and discussion

Initially, a single annulation of the corannulene nucleus [20] with benzothiophene was targeted (Scheme 1a). To accomplish this, ethynylcorannulene (**1**) [21] was subjected to a copper-catalyzed thiolation reaction in 85% isolated yield [22]. The Alkynyl sulfide (**2**) undergoes a cyclization reaction with an *in-situ* generated benzyne to furnish chloride **3** in 63% yield [23]. Having precursor **3** in hand, palladium-catalyzed intramolecular arylation was studied in the solution phase (Table 1) [24]. These reactions produced the targeted *peri*-annulated structure **4** in moderate yields (17%–39%) even after a long reaction time of 24 h at elevated temperatures (160 °C–200 °C). Thus, heating through microwave irradiation was investigated and found to enhance the yield of **4** significantly (up to 64%) in a reaction time of 1 h. To further raise product yield, the application of mechanochemistry became the focus of the investigation (Table 2) [25]. Initially, the catalyst and the base combination that had shown promising performance in the solution-phase reactions were employed. However, at room temperature, the reactions yielded no product. Increasing the reaction temperature to 150 °C resulted in a 6% yield. In searching for better conditions in the solid state, the nature of the base was changed from the liquid 1,8-diazabicyclo[5.4.0]undec-7-ene (DBU) to the solid Cs_2CO_3. This change produced the product in an improved yield of 46%. A further increase in the yield to 65% was achieved when the nature of the catalyst was changed to $Pd(OAc)_2$, known to perform well under ball milling conditions [12e,12r]. Subsequently, the effect of grinding auxiliaries on the reaction outcome was studied. Using NaCl as the grinding auxiliary resulted in a 91% yield, whereas KCl and LiCl yielded no product. To incorporate the selenium atom in the nanographene scaffold (Scheme 1b), a similar reaction sequence was carried out as described for the sulfur analogue (albeit with a change of diselenide as the electrophile due to its commercial availability) and resulted in alkynyl selenide **5** in 75% [26], chloride **6** in 33%, and *peri*-annulated **7** in 66% yield. Once again, the microwave-assisted reaction performed relatively poorly with an isolated yield of 53%.

Encouraged by these results, a twofold *peri*-annulation was then targeted (Figure 2a). For this, compound **8** was synthesized [27] and the trimethylsilyl groups were removed

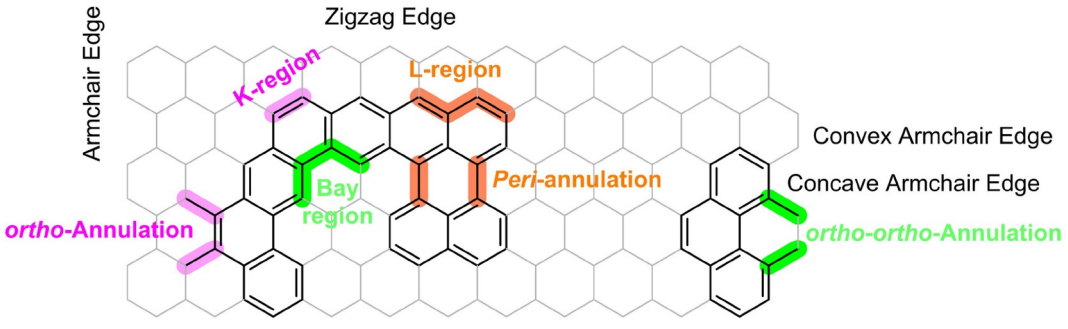

Figure 1 (Color online) Different types of nanographene edges and annulation chemistries.

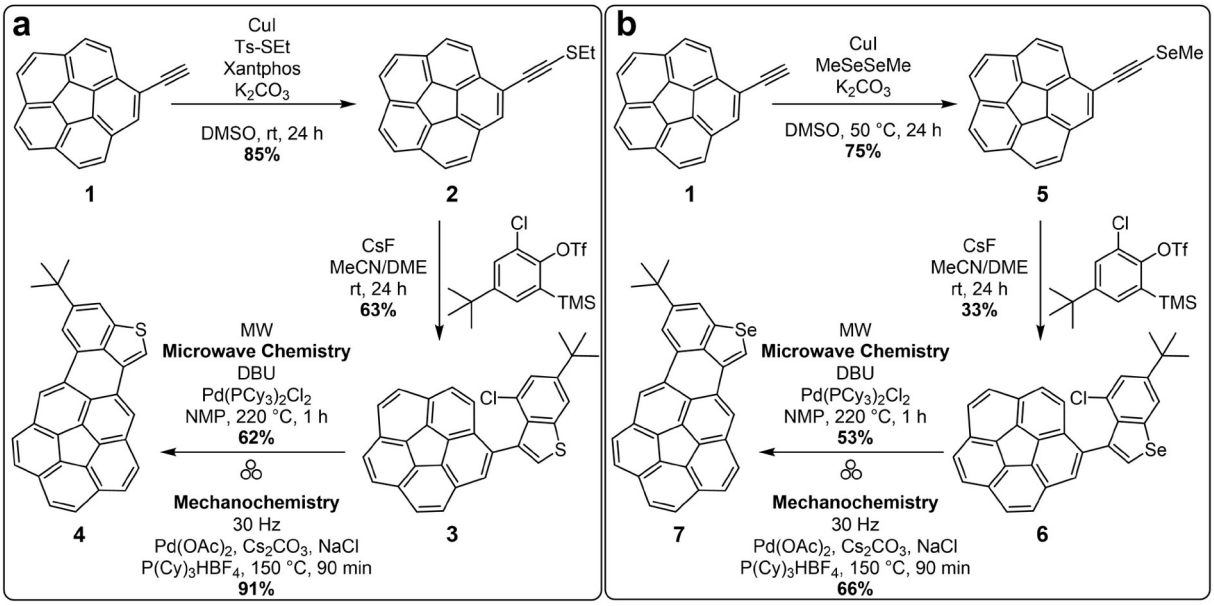

Scheme 1 *Peri*-annulation at the zigzag edge of corannulene. Synthesis of benzothiophene (a) and selenophene-based (b) bowl-shaped nanographenes.

Table 1 Optimization of the reaction conditions for the solution-phase synthesis of compound **4**. The entry in bold shows the optimum conditions

Entry	Catalyst	Ligand	Base	Solvent[a)]	Temp. & Time	Heating method	Yield (%)
1	$Pd(PCy_3)_2Cl_2$ (5%)	–	DBU (5 eq.)	DMF	160 °C, 24 h	oil bath	17
2	$Pd(PCy_3)_2Cl_2$ (5%)	–	DBU (5 eq.)	NMP	180 °C, 24 h	oil bath	26
3	$Pd(PCy_3)_2Cl_2$ (5%)	–	DBU (5 eq.)	NMP	200 °C, 24 h	oil bath	39
4	$Pd(PCy_3)_2Cl_2$ (5%)	–	DBU (5 eq.)	NMP	200 °C, 1 h	microwave	17
5	**$Pd(PCy_3)_2Cl_2$ (5%)**	–	**DBU (5 eq.)**	**NMP**	**220 °C, 1 h**	**microwave**	**62**
6	$Pd(PCy_3)_2Cl_2$ (5%)	–	DBU (5 eq.)	NMP	240 °C, 1 h	microwave	54
7	$Pd(OAc)_2$ (5%)	$P(Cy)_3 \cdot HBF_4$ (10%)	DBU (5 eq.)	NMP	220 °C, 1 h	microwave	49
8	$Pd(PCy_3)_2Cl_2$ (5%)	–	Cs_2CO_3 (5 eq.)	NMP	220 °C, 1 h	microwave	32

a) DBU = 1,8-Diazabicyclo[5.4.0]undec-7-ene, DMF = Dimethylformamide, NMP = *N*-Methylpyrrolidone.

Table 2 Optimization of reaction conditions for mechanosynthesis of compound **4**. The entry in bold shows optimum conditions

Entry	Catalyst	Ligand	Base	Grinding auxiliary	Temp. & Time	Yield (%)
1	$Pd(PCy_3)_2Cl_2$ (5%)	–	DBU (10 eq.)	–	rt, 90 min	0
2	$Pd(PCy_3)_2Cl_2$ (5%)	–	DBU (10 eq.)	–	150 °C, 90 min	6
3	$Pd(PCy_3)_2Cl_2$ (5%)	–	Cs_2CO_3 (10 eq.)	–	150 °C, 90 min	46
4	$Pd(OAc)_2$ (5%)	$P(Cy)_3 \cdot HBF_4$ (10%)	Cs_2CO_3 (10 eq.)	–	150 °C, 90 min	65
5	$Pd(OAc)_2$ (5%)	$P(Cy)_3 \cdot HBF_4$ (10%)	Cs_2CO_3 (10 eq.)	NaCl (1 g)	100 °C, 90 min	31
6	**$Pd(OAc)_2$ (5%)**	**$P(Cy)_3 \cdot HBF_4$ (10%)**	**Cs_2CO_3 (10 eq.)**	**NaCl (1 g)**	**150 °C, 90 min**	**91**
7	$Pd(OAc)_2$ (5%)	$P(Cy)_3 \cdot HBF_4$ (10%)	Cs_2CO_3 (10 eq.)	NaCl (1 g)	180 °C, 90 min	75
8	$Pd(OAc)_2$ (5%)	$P(Cy)_3 \cdot HBF_4$ (10%)	Cs_2CO_3 (10 eq.)	NaCl (1 g)	150 °C, 120 min	86
9	$Pd(OAc)_2$ (5%)	$P(Cy)_3 \cdot HBF_4$ (10%)	Cs_2CO_3 (10 eq.)	NaCl (1 g)	150 °C, 60 min	67
10	$PdCl_2$ (5%)	$P(Cy)_3 \cdot HBF_4$ (10%)	Cs_2CO_3 (10 eq.)	NaCl (1 g)	150 °C, 90 min	38
11	$Pd(OAc)_2$ (5%)	IPr·HCl (10%)	Cs_2CO_3 (10 eq.)	NaCl (1 g)	150 °C, 90 min	trace
12	$Pd(OAc)_2$ (5%)	$P(Cy)_3 \cdot HBF_4$ (10%)	Cs_2CO_3 (10 eq.)	KCl (1 g)	150 °C, 90 min	0
13	$Pd(OAc)_2$ (5%)	$P(Cy)_3 \cdot HBF_4$ (10%)	Cs_2CO_3 (10 eq.)	LiCl (1 g)	150 °C, 90 min	0

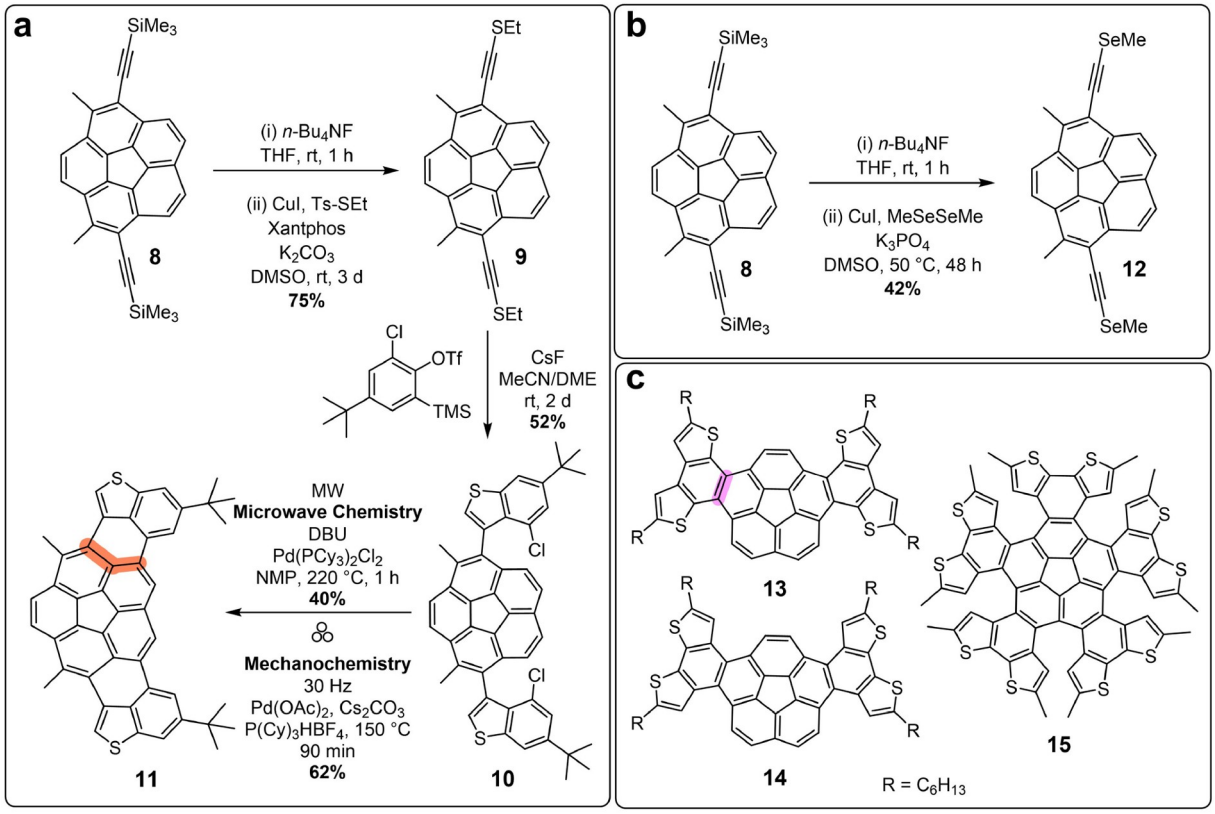

Figure 2 (Color online) (a) Bis-*peri*-annulation to give nanographene **11**. (b) Synthesis of bis-selenide precursor **12**. (c) Chemical structures of reported *ortho*-annulated benzothiophenes on a corannulene core for comparative purposes.

by treatment with tetrabutylammonium fluoride, followed by copper-catalyzed thiolation, resulting in compound **9** with an isolated yield of 75% (over two steps). Compound **10** was then synthesized via cyclization reaction with the benzyne precursor in 52% yield. Finally, nanographene **11** was obtained through twofold direct arylation reactions. The microwave-assisted reaction yielded 40% of the targeted product. The optimized reaction conditions for synthesizing the mono-annulated analogues in the solid state were applied by doubling the amounts of the catalyst, ligand, and base on precursor **10**. However, only trace amounts of the targeted product were isolated. This indicated that the optimum conditions for accessing mono-annulated products were not applicable for bis-annulation purposes and a separate optimization process was required (Table 3). Thus, the reaction time was extended to 6 h considering that a longer time may be required for the annulation to occur twice. However, this did not lead to any increase in the product yield. Once again, the grinding auxiliary (NaCl) was replaced with KCl or LiCl but did not help the reaction. Notably, however, when the grinding auxiliary was omitted, bis-*peri*-annulated nanographene **11** was obtained in 13% yield. By further optimizing the reaction time, the yield was improved to 61%. A selenide analogue of **11**, however, could not be prepared due to the instability of the bis-alkynyl-selenide compound **12** which was found to decompose during the subsequent cyclization reaction (Figure 2b).

Single crystals of **4**, suitable for X-ray diffraction analysis were obtained by the slow diffusion of ethanol into its bromobenzene solution (Figure 3). The single-crystal structure revealed one pair of enantiomers (**4-*V*** and **4-*X***), which arises from the bowl chirality of the molecule [17]. Both enantiomers exhibit an identical bowl depth of 0.92 Å. Along the *c*-axis, isomers ***V*** and ***X*** are arranged in columns, with each adopting a concave-to-concave and convex-to-convex packing orientation, respectively. In the *b*-axis view, the ***V*** and ***X*** isomers are organized in an alternating layer pattern with the same π-π distance of 3.28 Å. Single crystals of **11** suitable for X-ray diffraction analysis were obtained by slowly diffusing methanol into its chlorobenzene solution (Figure 4). Nanographene **11** exhibits a bowl depth of 0.90 Å. The molecules are arranged in a slip-stacked column, with the bowl orientations aligned in the same direction along the stack in the single crystal of **11**.

The UV-Vis absorption spectra of these compounds were measured in dichloromethane (DCM) at a concentration of 10^{-5} mol/L (Table 4 and Figure 5). The spectra of the sulfur-doped compound (**4**) and selenium-doped compound (**7**) are observed to be similar, with compound **4** exhibiting a higher molar absorption coefficient than compound **7**, which also

Table 3 Optimization of the reaction conditions for mechanosynthesis of compound **11.** The entry in bold shows the optimum conditions

Entry	Catalyst	Ligand	Base	Grinding auxiliary	Temp. & Time	Yield (%)
1	$Pd(OAc)_2$ (10%)	$P(Cy)_3{\cdot}HBF_4$ (20%)	Cs_2CO_3 (20 eq.)	NaCl (1 g)	150 °C, 90 min	trace
2	$Pd(OAc)_2$ (10%	$P(Cy)_3{\cdot}HBF_4$ (20%)	Cs_2CO_3 (20 eq.)	NaCl (1 g)	150 °C, 6 h	trace
3	$Pd(OAc)_2$ (10%)	$P(Cy)_3{\cdot}HBF_4$ (20%)	Cs_2CO_3 (20 eq.)	–	150 °C, 90 min	13
4	$Pd(OAc)_2$ (10%)	$P(Cy)_3{\cdot}HBF_4$ (20%)	Cs_2CO_3 (20 eq.)	–	150 °C, 2 h	22
5	$Pd(OAc)_2$ (10%)	$P(Cy)_3{\cdot}HBF_4$ (20%)	Cs_2CO_3 (20 eq.)	–	150 °C, 2.5 h	45
6	**$Pd(OAc)_2$ (10%)**	**$P(Cy)_3{\bullet}HBF_4$ (20%)**	**Cs_2CO_3 (20 eq.)**	–	**150 °C, 3 h**	**61**
7	$Pd(OAc)_2$ (10%)	$P(Cy)_3{\cdot}HBF_4$ (20%)	Cs_2CO_3 (20 eq.)	–	150 °C, 3.5 h	58
8	$Pd(OAc)_2$ (10%)	$P(Cy)_3{\cdot}HBF_4$ (20%)	Cs_2CO_3 (20 eq.)	KCl (1 g)	150 °C, 90 min	0
9	$Pd(OAc)_2$ (10%)	$P(Cy)_3{\cdot}HBF_4$ (20%)	Cs_2CO_3 (20 eq.)	LiCl (1 g)	150 °C, 90 min	0

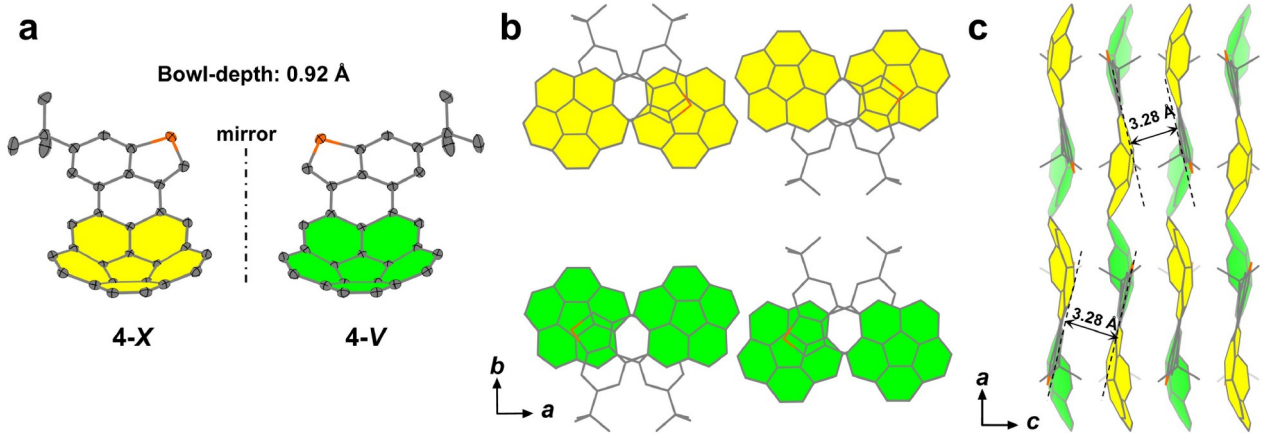

Figure 3 (Color online) Single-crystal structure of **4**. (a) ORTEP representation of single molecular structure (50% probability ellipsoids). Molecular packing structures: top view (b) and side view (c). The bowl-depth values are defined by the distance between the centroid of the central five-membered ring and the mean plane of the ten carbon atoms on the rim. All the hydrogen atoms, solvent molecules and disordered atoms are omitted for clarity.

shows a slight redshift compared to **4**. Compound **4** has a maximum absorption at 442 nm with a molar absorption coefficient of 2.0×10^4 M^{-1} cm^{-1}, while compound **7** has a maximum at 446 nm with a coefficient of 1.9×10^4 M^{-1} cm^{-1}. Compound **11** absorbs maximally at 416 nm with a molar absorption coefficient of 2.3×10^4 M^{-1} cm^{-1}. In comparison to **4** and **7** ($\lambda_{edge} \approx 475$ nm), the absorption range of **11** extends upto 500 nm.

Photoluminescence (PL) measurements were taken for compounds **4**, **7**, and **11**, through excitation at 418, 422, and 416 nm, yielding fluorescence quantum yields of 14.1%, 0.4%, and 9.1%, respectively. To investigate the electrochemical properties, cyclic voltammetry (CV) and square-wave voltammograms (SWV) were performed in anhydrous dichloromethane with 0.1 M *n*-Bu_4NPF_6 as the electrolyte (Figure 6). Potentials were calibrated using the Fc/Fc^+ redox couple (4.8 eV below the vacuum level), allowing calculation of energy levels from the onset oxidation and reduction potentials. The highest occupied molecular orbitals (HOMO) of compounds **4** and **7** are similar, at −5.31 and −5.32 eV, respectively. The lowest unoccupied molecular orbital (LUMO) of compound **4** is −2.64 eV, higher than the LUMO of **7** at −2.80 eV. The HOMO and LUMO of compound **11** are −5.17 and −2.78 eV, respectively.

The effect of *peri*-annulation on molecular properties can be gauged by comparison with known systems in which the aromatic extension of the corannulene nucleus occurs through *ortho*-annulation. Compounds **13**, **14**, and **15** are all of interest in this regard (Figure 2c) [28,29]. The core in all these cases is extended through *ortho*-annulation of *K*-regions. However, while on one hand the benzothiophene is not connected to the core via its 3,4-positions in these molecules, the extent of aromatic area extension is larger due to the presence of a second thiophene ring in the structure. Furthermore, in **15**, this π-extension occurs five times. Thus, **13**–**15** are larger π-systems in terms of the number of electronically conjugated sp^2-carbon atoms (column 2 in Table 4). It is interesting to observe, therefore, that **4** exhibits a >100 nm red-shift in its absorption spectrum as compared to **13** and **14** (Table 4). The optical band gap for **4** is smaller

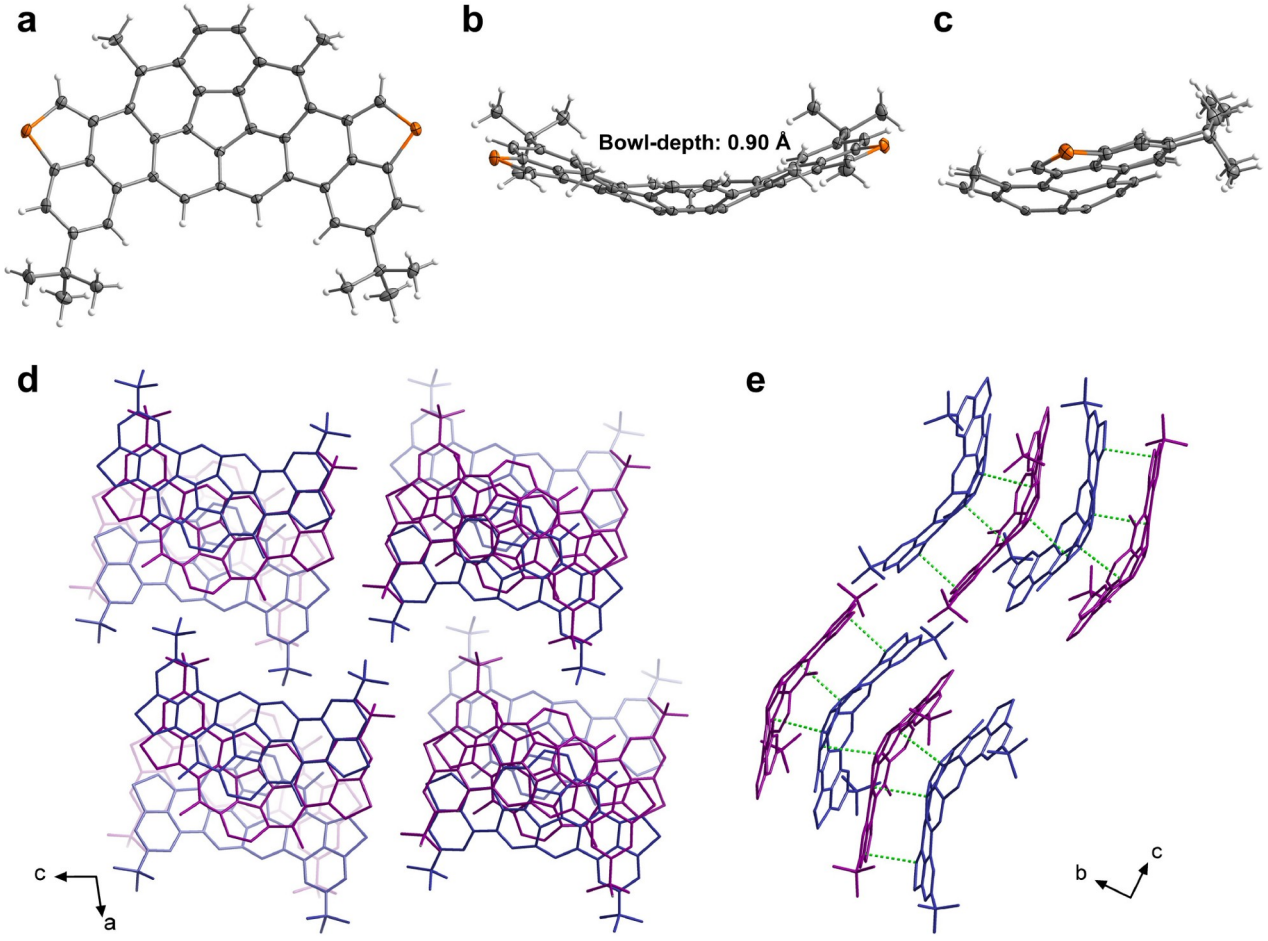

Figure 4 (Color online) Single-crystal structure of **11**. ORTEP representation of single molecular structures (50% probability ellipsoids): top view (a) and side views (b, c). Molecular packing structures: top view (d) and side view (e). All the hydrogen atoms, solvent molecules and disordered atoms are omitted for clarity.

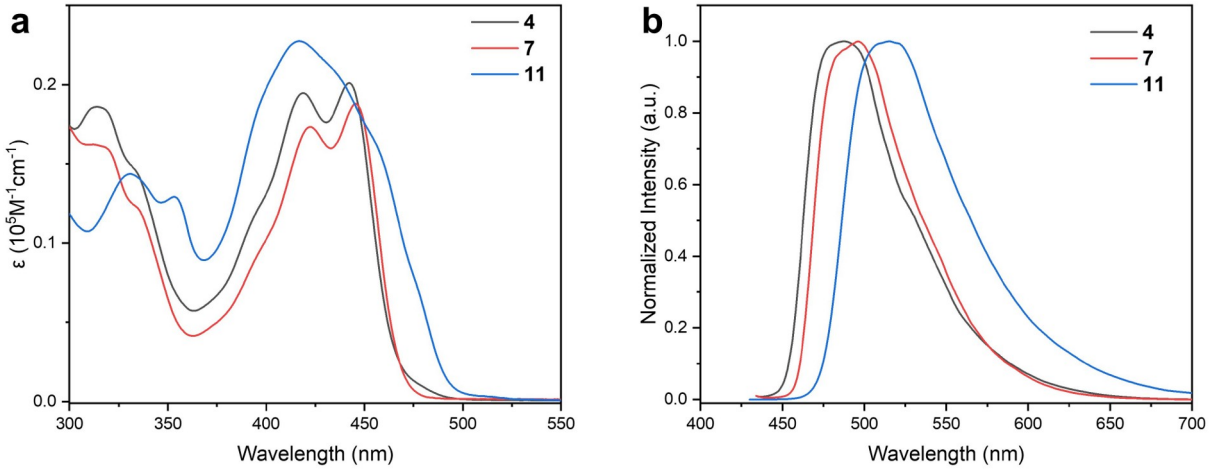

Figure 5 (Color online) (a) The UV-Vis absorption spectra of **4**, **7**, and **11** in dichloromethane with a concentration of 1.0×10^{-5} mol L^{-1}. (b) Normalized photoluminescence spectra of **4**, **7**, and **11** in dichloromethane with a concentration of 1.0×10^{-4} mol L^{-1} and excitation at 418, 422, and 416 nm, respectively.

than **13** and **14** by 0.16 and 0.21 eV, respectively. The HOMO energy levels of compounds **13** and **14** are lower than the HOMO energy level of compound **4**. Meanwhile, besides showing a 46–72 nm bathochromic shift in the absorption spectra, **4** and **11** both show several times higher quantum yield of emission than **15**. Thus, *peri*-annulation

Table 4 Optoelectronic properties of the nanographenes

Compound	sp^2 Carbon Atoms	λ_{max}(abs) (nm)	ε (M^{-1} cm^{-1})	E_{opt} (eV)[a)]	λ_{em} (nm)	QY (%)	HOMO (eV)[b)]	LUMO (eV)[c)]
4	28	442	2.0×10^4	2.60	487	14.1	−5.31	−2.64
7	28	446	1.9×10^4	2.62	496	0.4	−5.32	−2.80
11	36	416	2.3×10^4	2.51	514	9.1	−5.17	−2.78
13[28]	36	335	–	2.76	–	–	−5.59	–
14[28]	36	323	–	2.87	–	–	−5.65	–
15[29]	60	370	–	–	502	2.0	–	–

a) Optical band gaps were estimated from the onset of absorption; b) $E_{HOMO} = -(4.8\ eV - E_{onset}^{1st\ red})$; c) $E_{LUMO} = -(4.8\ eV - E_{onset}^{1st\ oxid})$.

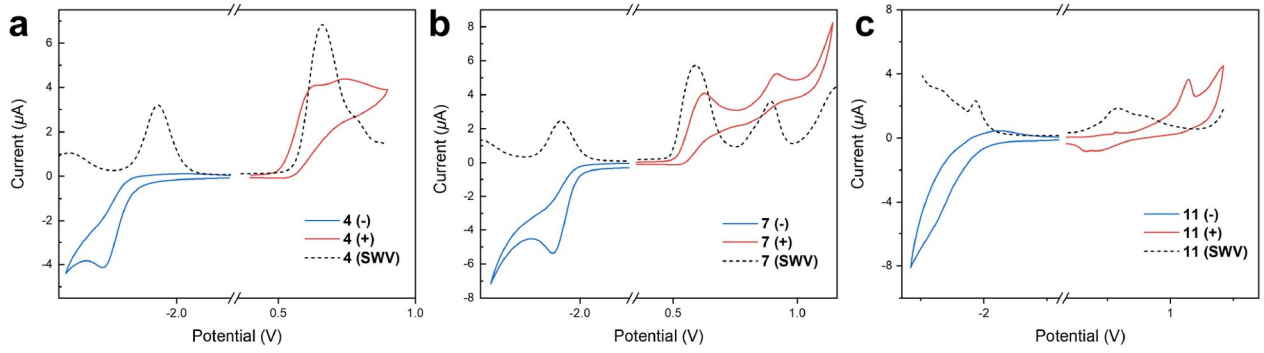

Figure 6 (Color online) Cyclic voltammograms (solid line) and square-wave voltammograms (dash line) of **4** (a), **7** (b), and **11** (c) in DCM (1 mmol L^{-1}) containing 0.1 M *n*-Bu_4NPF_6.

appears to be a valuable molecular motif in the design of nanographene materials with attractive optoelectronic properties.

3 Conclusions

In conclusion, mechanochemistry is a valuable synthetic tool in accessing *peri*-annulated polyarenes through palladium-catalyzed intramolecular arylation reactions. This method is superior to the solution phase and the microwave-assisted reactions. It allows synthetic access to challenging curved nanostructures in isolated yields of 62%–91%. Among other benefits, an economical palladium source, $Pd(OAc)_2$, is found to be effective as the catalyst. The synthesized structures contain sulfur and selenium atoms and exhibit better optoelectronic properties than other related structures due to the nature of the annulation chemistry. Overall, the results indicate the potential of mechanochemical reactions in accessing *peri*-annulated molecular graphene structures with appealing properties.

Acknowledgements This work was supported by the Ministry of Education Singapore under the AcRF Tier 2 (MOE-T2EP10221-0002) and the Ministry of Research, Innovation and Digitalization under Romania's National Recovery and Resilience Plan PNRR-III-C9- 2022–I8 Program with Project code 167/15.11.22.

Conflict of interest The authors declare no conflict of interest.

Supporting information The supporting information is available online at http://chem.scichina.com and http://link.springer.com/journal/11426. The supporting materials are published as submitted, without typesetting or editing. The responsibility for scientific accuracy and content remains entirely with the authors.

1 (a) James SL, Adams CJ, Bolm C, Braga D, Collier P, Friščić T, Grepioni F, Harris KDM, Hyett G, Jones W, Krebs A, Mack J, Maini L, Orpen AG, Parkin IP, Shearouse WC, Steed JW, Waddell DC. *Chem Soc Rev*, 2012, 41: 413–447; (b) Howard JL, Brand MC, Browne DL. *Angew Chem*, 2018, 130: 16336–16340; (c) Howard JL, Sagatov Y, Repusseau L, Schotten C, Browne DL. *Green Chem*, 2017, 19: 2798–2802; (d) Andersen J, Mack J. *Green Chem*, 2018, 20: 1435–1443; (e) Bolm C, Hernández JG. *ChemSusChem*, 2018, 11: 1410–1420; (f) Colacino E, Porcheddu A, Charnay C, Delogu F. *React Chem Eng*, 2019, 4: 1179–1188; (g) Friščić T, Mottillo C, Titi HM. *Angew Chem*, 2020, 132: 1030–1041; (h) Gečiauskaitė AA, García F. *Beilstein J Org Chem*, 2017, 13: 2068–2077; (i) Pickhardt W, Grätz S, Borchardt L. *Chem Eur J*, 2020, 26: 12903–12911; (j) Ralphs K, Hardacre C, James SL. *Chem Soc Rev*, 2013, 42: 7701–7718; (k) Rodríguez B, Bruckmann A, Rantanen T, Bolm C. *Adv Synth Catal*, 2007, 349: 2213–2233; (l) Tan D, García F. *Chem Soc Rev*, 2019, 48: 2274–2292; (m) Howard JL, Cao Q, Browne DL. *Chem Sci*, 2018, 9: 3080–3094; (n) Wang GW. *Chem Soc Rev*, 2013, 42: 7668–7700

2 (a) Do JL, Friščić T. *ACS Cent Sci*, 2017, 3: 13–19; (b) Hernández JG,

Bolm C. *J Org Chem*, 2017, 82: 4007–4019; (c) Cuccu F, De Luca L, Delogu F, Colacino E, Solin N, Mocci R, Porcheddu A. *ChemSusChem*, 2022, 15: e202200362
3 (a) Yong T, Báti G, García F, Stuparu MC. *Nat Commun*, 2021, 12: 5187; (b) Báti G, Laxmi S, Stuparu MC. *ChemSusChem*, 2023, 16: e202301087
4 Crawford D, Casaban J, Haydon R, Giri N, McNally T, James SL. *Chem Sci*, 2015, 6: 1645–1649
5 (a) Crawford DE, Wright LA, James SL, Abbott AP. *Chem Commun*, 2016, 52: 4215–4218; (b) Martina K, Rotolo L, Porcheddu A, Delogu F, Bysouth SR, Cravotto G, Colacino E. *Chem Commun*, 2018, 54: 551–554; (c) Crawford DE, Porcheddu A, McCalmont AS, Delogu F, James SL, Colacino E. *ACS Sustain Chem Eng*, 2020, 8: 12230–12238
6 Teoh Y, Ayoub G, Huskić I, Titi HM, Nickels CW, Herrmann B, Friščić T. *Angew Chem Int Ed*, 2022, 61: e202206293
7 (a) Fulmer DA, Shearouse WC, Medonza ST, Mack J. *Green Chem*, 2009, 11: 1821–1825; (b) Cook TL, Walker JA, Mack J. *Green Chem*, 2013, 15: 617–619; (c) Vogt CG, Grätz S, Lukin S, Halasz I, Etter M, Evans JD, Borchardt L. *Angew Chem Int Ed*, 2019, 58: 18942–18947; (d) Grätz S, Oltermann M, Vogt CG, Borchardt L. *ACS Sustain Chem Eng*, 2020, 8: 7569–7573; (e) Kong D, Amer MM, Bolm C. *Green Chem*, 2022, 24: 3125–3129; (f) Kong D, Bolm C. *Green Chem*, 2022, 24: 6476–6480; (g) Pickhardt W, Beaković C, Mayer M, Wohlgemuth M, Kraus FJL, Etter M, Grätz S, Borchardt L. *Angew Chem Int Ed*, 2022, 61: e202205003
8 (a) Friščić T, Trask AV, Jones W, Motherwell WDS. *Angew Chem Int Ed*, 2006, 45: 7546–7550; (b) Belenguer AM, Friščić T, Day GM, Sanders JKM. *Chem Sci*, 2011, 2: 696–700; (c) Bowmaker GA. *Chem Commun*, 2013, 49: 334–348; (d) Chen L, Regan M, Mack J. *ACS Catal*, 2016, 6: 868–872; (e) Cao Q, Howard JL, Crawford DE, James SL, Browne DL. *Green Chem*, 2018, 20: 4443–4447
9 (a) Andersen J, Mack J. *Angew Chem Int Ed*, 2018, 57: 13062–13065; (b) Andersen J, Brunemann J, Mack J. *React Chem Eng*, 2019, 4: 1229–1236; (c) Cindro N, Tireli M, Karadeniz B, Mrla T, Užarević K. *ACS Sustain Chem Eng*, 2019, 7: 16301–16309
10 Bolm C, Hernández JG. *Angew Chem Int Ed*, 2019, 58: 3285–3299
11 (a) Zhang P, Dai S. *J Mater Chem A*, 2017, 5: 16118–16127; (b) Kubota K, Ito H. *Trends Chem*, 2020, 2: 1066–1081
12 (a) Ravnsbæk JB, Swager TM. *ACS Macro Lett*, 2014, 3: 305–309; (b) Puccetti F, Schumacher C, Wotruba H, Hernández JG, Bolm C. *ACS Sustain Chem Eng*, 2020, 8: 7262–7266; (c) Xuan M, Schumacher C, Bolm C, Göstl R, Herrmann A. *Adv Sci*, 2022, 9: 2105497; (d) Ardila-Fierro KJ, Bolm C, Hernández JG. *Angew Chem Int Ed*, 2019, 58: 12945–12949; (e) Báti G, Csókás D, Yong T, Tam SM, Shi RRS, Webster RD, Pápai I, García F, Stuparu MC. *Angew Chem Int Ed*, 2020, 59: 21620–21626; (f) Wang C, Sun Q, García F, Wang C, Yoshikai N. *Angew Chem Int Ed*, 2021, 60: 9627–9634; (g) Yuan Y, Wang T, Chen H, Mahurin SM, Luo H, Veith GM, Yang Z, Dai S. *Angew Chem Int Ed*, 2020, 59: 21935–21939; (h) Shayesteh K, Moghaddas J, Haghighi M, Eskandari H. *Asian J Chem*, 2010, 22: 2106–2116; (i) Kubota K, Baba E, Seo T, Ishiyama T, Ito H. *Beilstein J Org Chem*, 2022, 18: 855–862; (j) Grätz S, Beyer D, Tkachova V, Hellmann S, Berger R, Feng X, Borchardt L. *Chem Commun*, 2018, 54: 5307–5310; (k) Báti G, Csókás D, Stuparu MC. *Chem Eur J*, 2024, 30: e202302971; (l) Hum G, Muzammil EM, Li Y, García F, Stuparu MC. *Chem Eur J*, 2024, 30: e202402056; (m) Toda F, Tanaka K, Iwata S. *J Org Chem*, 1989, 54: 3007–3009; (n) Fujishiro K, Morinaka Y, Ono Y, Tanaka T, Scott LT, Ito H, Itami K. *J Am Chem Soc*, 2023, 145: 8163–8175; (o) Seo T, Kubota K, Ito H. *J Am Chem Soc*, 2023, 145: 6823–6837; (p) Seo T, Toyoshima N, Kubota K, Ito H. *J Am Chem Soc*, 2021, 143: 6165–6175; (q) Zhao Y, Rocha SV, Swager TM. *J Am Chem Soc*, 2016, 138: 13834–13837; (r) Stanojkovic J, William R, Zhang Z, Fernández I, Zhou J, Webster RD, Stuparu MC. *Nat Commun*, 2023, 14: 803; (s) Krusenbaum A, Grätz S, Bimmermann S, Hutsch S, Borchardt L. *RSC Adv*, 2020, 10: 25509–25516; (t) Baier DM, Grätz S, Jahromi BF, Hellmann S, Bergheim K, Pickhardt W, Schmid R, Borchardt L. *RSC Adv*, 2021, 11: 38026–38032; (u) Wang C, Hill M, Theard B, Mack J. *RSC Adv*, 2019, 9: 27888–27891; (v) Rasmussen MO, Axelsson O, Tanner D. *Synth Commun*, 1997, 27: 4027–4030
13 (a) Ma Z, Winands T, Liang N, Meng D, Jiang W, Doltsinis NL, Wang Z. *Sci China Chem*, 2020, 63: 208–214; (b) Wang XY, Yao X, Müllen K. *Sci China Chem*, 2019, 62: 1099–1144; (c) Zheng C, Zhu J, Yang C, Lu C, Chen Z, Zhuang X. *Sci China Chem*, 2019, 62: 1145–1193; (d) Gong ZL, Zhu X, Zhou Z, Zhang SW, Yang D, Zhao B, Zhang YP, Deng J, Cheng Y, Zheng YX, Zang SQ, Kuang H, Duan P, Yuan M, Chen CF, Zhao YS, Zhong YW, Tang BZ, Liu M. *Sci China Chem*, 2021, 64: 2060–2104; (e) Ma S, Zhu Y, Dou W, Chen Y, He X, Wang J. *Sci China Chem*, 2021, 64: 576–580; (f) Xu Q, Wang C, Zheng D, Wang Y, Chen X, Sun D, Jiang H. *Sci China Chem*, 2021, 64: 590–598; (g) Zhang M, Bai Y, Sun C, Xue L, Wang H, Zhang ZG. *Sci China Chem*, 2021, 65: 462–485; (h) Chen K, Chen X, Hu K, Zhao Y, Liu Y, Liu G, Chen J, Jiang W, Shuai Z, Qu DH, Wang Z. *Sci China Chem*, 2024, 67: 1324–1333; (i) Zhang L, Qiu S, Hu S, Xu H, Sun X, Jiang W, Qu D, Wang Z. *Sci China Chem*, 2025, 68, https://doi.org/10.1007/s11426-024-2474-6; (j) Liu P, Li Y, Wu MX, Kang H, Zhao XL, Xu L, Liu L, Li X, Fang J, Fang Z, Cheng Y, Yang HB, Yu H, Shi X. *Sci China Chem*, 2025, 68: 233–240
14 (a) Pozo I, Guitián E, Pérez D, Peña D. *Acc Chem Res*, 2019, 52: 2472–2481; (b) Pun SH, Miao Q. *Acc Chem Res*, 2018, 51: 1630–1642; (c) Wang XY, Yao X, Narita A, Müllen K. *Acc Chem Res*, 2019, 52: 2491–2505; (d) Zhu Y, Wang J. *Acc Chem Res*, 2023, 56: 363–373; (e) Grzybowski M, Sadowski B, Butenschön H, Gryko DT. *Angew Chem Int Ed*, 2020, 59: 2998–3027; (f) Grzybowski M, Skonieczny K, Butenschön H, Gryko DT. *Angew Chem Int Ed*, 2013, 52: 9900–9930; (g) Liu J, Feng X. *Angew Chem Int Ed*, 2020, 59: 23386–23401; (h) Majewski MA, Stępień M. *Angew Chem Int Ed*, 2019, 58: 86–116; (i) Stępień M, Gońka E, Żyła M, Sprutta N. *Chem Rev*, 2017, 117: 3479–3716; (j) Zhang Y, Pun SH, Miao Q. *Chem Rev*, 2022, 122: 14554–14593; (k) Narita A, Wang XY, Feng X, Müllen K. *Chem Soc Rev*, 2015, 44: 6616–6643; (l) Gu Y, Qiu Z, Müllen K. *J Am Chem Soc*, 2022, 144: 11499–11524; (m) Liu YM, Hou H, Zhou YZ, Zhao XJ, Tang C, Tan YZ, Müllen K. *Nat Commun*, 2018, 9: 1901; (n) Tan YZ, Yang B, Parvez K, Narita A, Osella S, Beljonne D, Feng X, Müllen K. *Nat Commun*, 2013, 4: 2646; (o) Magiera KM, Aryal V, Chalifoux WA. *Org Biomol Chem*, 2020, 18: 2372–2386; (p) Anderson HV, Gois ND, Chalifoux WA. *Org Chem Front*, 2023, 10: 4167–4197; (q) Kawasumi K, Zhang Q, Segawa Y, Scott LT, Itami K. *Nat Chem*, 2013, 5: 739–744; (r) Zhang K, Chen Z-C, Wu Y-F, Tian H-R, Zhang L, Zhang M-L, Deng S-L, Zhang Q, Xie S-Y, Zheng L-S. *Angew Chem Int Ed*, 2024, 31: e202417269; (s) Zhang XP, Ying SW, Zhang YL, Zhang WX, Shi W, Chen BW, Tian HR, Xu G, Wang SS, Zhang Q, Xie SY, Zheng LS. *J Am Chem Soc*, 2024, 146: 30913–30921
15 (a) Tsvetkov NP, Gonzalez-Rodriguez E, Hughes A, dos Passos Gomes G, White FD, Kuriakose F, Alabugin IV. *Angew Chem Int Ed*, 2018, 57: 3651–3655; (b) Shen T, Zou Y, Hou X, Wei H, Ren L, Jiao L, Wu J. *Angew Chem Int Ed*, 2023, 62: e202311928; (c) Yang W, Bam R, Catalano VJ, Chalifoux WA. *Angew Chem Int Ed*, 2018, 57: 14773–14777; (d) Yang X, Rominger F, Mastalerz M. *Angew Chem Int Ed*, 2021, 60: 7941–7946; (e) Shoyama K, Mahl M, Seifert S, Würthner F. *J Org Chem*, 2018, 83: 5339–5346; (f) Gonzalez-Rodriguez E, Abdo MA, dos Passos Gomes G, Ayad S, White FD, Tsvetkov NP, Hanson K, Alabugin IV. *J Am Chem Soc*, 2020, 142: 8352–8366; (g) Lungerich D, Papaianina O, Feofanov M, Liu J, Devarajulu M, Troyanov SI, Maier S, Amsharov K. *Nat Commun*, 2018, 9: 4756; (h) Shoyama K, Schmidt D, Mahl M, Würthner F. *Org Lett*, 2017, 19: 5328–5331; (i) Fernández-García JM, Evans PJ, Medina Rivero S, Fernández I, García-Fresnadillo D, Perles J, Casado J, Martín N. *J Am Chem Soc*, 2018, 140: 17188–17196
16 (a) Jackson EA, Steinberg BD, Bancu M, Wakamiya A, Scott LT. *J Am Chem Soc*, 2007, 129: 484–485; (b) Lampart S, Roch LM, Dutta AK, Wang Y, Warshamanage R, Finke AD, Linden A, Baldridge KK, Siegel JS. *Angew Chem Int Ed*, 2016, 55: 14648–14652; (c) Xu Q,

Wang C, Zhao Y, Zheng D, Shao C, Guo W, Deng X, Wang Y, Chen X, Zhu J, Jiang H. *Org Lett*, 2020, 22: 7397–7402; (d) Zhu ZZ, Chen ZC, Yao YR, Cui CH, Li SH, Zhao XJ, Zhang Q, Tian HR, Xu PY, Xie FF, Xie XM, Tan YZ, Deng SL, Quimby JM, Scott LT, Xie SY, Huang RB, Zheng LS. *Sci Adv*, 2019, 5: eaaw0982
17 Zhang Z, Csókás D, Fernández I, Stuparu MC. *Chem*, 2024, 10: 3199–3211
18 (a) Markiewicz JT, Wudl F. *ACS Appl Mater Interfaces*, 2015, 7: 28063–28085; (b) Chen L, Li C, Müllen K. *J Mater Chem C*, 2014, 2: 1938–1956; (c) Shoyama K, Würthner F. *Org Chem Front*, 2025, 12: 328–345
19 Rieger R, Müllen K. *J Phys Org Chem*, 2010, 23: 315–325
20 (a) Stuparu MC. *Acc Chem Res*, 2021, 54: 2858–2870; (b) Nestoros E, Stuparu MC. *Chem Commun*, 2018, 54: 6503–6519; (c) Tsefrikas VM, Scott LT. *Chem Rev*, 2006, 106: 4868–4884; (d) Wu YT, Siegel JS. *Chem Rev*, 2006, 106: 4843–4867; (e) Muzammil EM, Halilovic D, Stuparu MC. *Commun Chem*, 2019, 2: 58; (f) Sygula A. *Eur J Org Chem*, 2011, 2011: 1611–1625
21 Jones CS, Elliott E, Siegel JS. *Synlett*, 2004, 1: 187–191
22 Kanemoto K, Yoshida S, Hosoya T. *Org Lett*, 2019, 21: 3172–3177
23 Matsuzawa T, Hosoya T, Yoshida S. *Chem Sci*, 2020, 11: 9691–9696
24 Hagui W, Doucet H, Soulé JF. *Chem*, 2019, 5: 2006–2078
25 Yang X, Wu C, Su W, Yu J. *Eur J Org Chem*, 2022, 2022: e202101440
26 Bieber LW, da Silva MF, Menezes PH. *Tetrahedron Lett*, 2004, 45: 2735–2737
27 Wu YT, Bandera D, Maag R, Linden A, Baldridge KK, Siegel JS. *J Am Chem Soc*, 2008, 130: 10729–10739
28 Lu RQ, Zhou YN, Yan XY, Shi K, Zheng YQ, Luo M, Wang XC, Pei J, Xia H, Zoppi L, Baldridge KK, Siegel JS, Cao XY. *Chem Commun*, 2015, 51: 1681–1684
29 Lin HA, Kato K, Segawa Y, Scott LT, Itami K. *Chem Sci*, 2019, 10: 2326–2330